Environmental Science and Pollution Research (2020) 27:6589–6602
https://doi.org/10.1007/s11356-019-07310-4

RESEARCH ARTICLE

Assessment of spring water quality and associated health risks in a high-level natural radiation area, North Iran

Farideh Amini Birami[1] · Farid Moore[1] · Reza Faghihi[2] · Behnam Keshavarzi[1]

Received: 13 July 2019 / Accepted: 5 December 2019 / Published online: 24 December 2019

Abstract

In this study, the spring water quality of a high natural background radiation region in North Iran was evaluated by measuring hydrochemical characteristics and concentration of potentially toxic elements (PTEs) and activity concentration of radioactive elements. The carcinogenicity potential from exposure to PTEs and radioactive elements was also investigated using probabilistic approach. The hydrochemical properties of water samples revealed that there were two different water types in the study area: (1) non-thermal Ca-HCO3 type and (2) thermal Na-Cl type. The concentrations of Al, Cd, Cr, Cu, Pb, Mo, Ni, Sb, Zn, and ^{40}K were within the recommended water quality standard set by the World Health Organization (WHO). Elevated concentrations of As, Mn, Hg, ^{226}Ra, and ^{232}Th occur in Na-Cl water type while elevated concentrations of Fe occur in Ca-HCO_3 water type. Also, health complications of dermal contact (via balneology or bathing) are within the safe limits. The major concern regarding the contaminated springs is the possibility of soil and groundwater contamination through uncontrolled runoff and spa effluents. Preventing the spread of toxic constituents in the study area via high-risk spring water requires periodic monitoring, and applying control measures where necessary.

Keywords Spring water · Potentially toxic elements · Radioactive elements · Health hazard · Ramsar

Introduction

Spring water is an important environmental indicator as its quality varies depending on physical, chemical, and biological characteristics of the media through which the water passes (Jasik et al. 2017). Among a long list of parameters that affect spring water quality, the occurrence of potentially toxic elements (PTEs) and radioactive elements are the prime focus of environmental scientists due to their toxic nature, especially where they occur in excess of regulatory standard concentrations (Benedik et al. 2015; Huq et al. 2019). Dissolved elements in spring water are significantly affected by geogenic sources such as ore deposits, soil leaching, hydrothermal activity, and weathering processes (Amarouche-Yala et al. 2015; El-Gamal et al. 2018; Wang et al. 2016) on top of anthropogenic activities such as industrial and domestic effluents, nuclear accident, and fission products of nuclear testing (Lien et al. 2019; Papaefthymiou et al. 2007). These elemental contaminants of spring water may enter the human body through various pathways, including direct ingestion and dermal contact during washing, swimming, and taking shower (USEPA 2016). On the other hand, water discharged from heavily contaminated springs may deposit high concentration of chemical compounds at and near the discharge area. These deposits are apt to become significant sources of contamination for groundwater and soil. Therefore, it is essential to assess the health concerns that such springs impose in order to achieve effective water management. There are many springs in the North of Iran, flowing between Chaboksar city in Gilan province and Ramsar, Tonekabon, and Kelardasht in Mazandaran province. These springs are commonly used by locals and tourists for drinking, irrigation, bathing, and therapeutic purposes. Moreover, spring runoffs flow through

Responsible editor: Philippe Garrigues

Electronic supplementary material The online version of this article (https://doi.org/10.1007/s11356-019-07310-4) contains supplementary material, which is available to authorized users.

✉ Farid Moore
moore@shirazu.ac.ir

[1] Department of Earth Sciences, College of Sciences, Shiraz University, Shiraz, Iran

[2] Department of Nuclear Engineering, School of Mechanical Engineering, Shiraz University, Shiraz, Iran

populated rural and agricultural areas with no mitigation and adaptation strategies. Therefore, their infiltration into soil and shallow water tables may pose a serious threat to public health. The study area is a matter of great concern, as it has the highest natural radioactivity levels among all high-level radiation areas in the world (Khademi and Tahsili 1972). Thus, many dosimetric and radiobiological studies have already been conducted in this area, and the results exhibited that local inhabitants are continuously subjected to high radiation doses as a result of terrestrial gamma radiation and ^{222}Rn gas inhalation (Fathabadi et al. 2017; Mortazavi and Mozdarani 2013; Sohrabi and Babapouran 2005). However, despite many reported elevated levels of radioactive elements in various parts of the study area, a limited number of springs have been investigated for this purpose (Ansari et al. 2011; Mortazavi and Mozdarani 2013). Furthermore, the threat posed by PTEs has largely been neglected. Keeping these gaps in view, the results of this study could provide useful information for the local government official to take sound decisions on water risk management plans. The objectives of the present study are the following: (a) to evaluate the spatial distribution of PTEs (As, Cd, Cr, Cu, Fe, Hg, Mn, Mo, Ni, Pb, Sb, and Zn) as well as radioactive elements (^{226}Ra, ^{232}Th, and ^{40}K) throughout the sampling stations; (b) to reveal possible sources and factors that control the concentrations of these elements; and (c) to evaluate the risk they pose to human health.

Materials and methods

Description of the study area

The study area between the Alborz Mountains and the Caspian Sea is a vegetation-covered district that lies between N 36° 59′ to N 36° 21′ and E 50 °30′ to E 51° 12′ (Fig. 1). Climatically, the area practices humid to subhumid subtropical climate (Roozitalab et al. 2018). The mean annual rainfall is about 1500 mm that mostly occurs in autumn, and the mean annual temperature is 16 °C. The hottest month of the year is August (mean temperature 25 °C) and the coldest is February (mean temperature 7 °C). The northern coastal plain aquifer comprises four hydrogeological units from surface to depth as follows: (1) a shallow unconfined aquifer composed of sand and gravel and calcareous material; (2) an aquitard composed of clay and silty clay; (3) an aquifer composed of fine to medium-sized sand and gravel; and (4) a poorly transmissive unit of marine sandy and silty sediments saturated with paleo-brackish waters (Alavi 1996).

Geologically, the study area is part of the so called Central Alborz zone. The Alborz zone separated from the Gondwana plate during Ordovician to Silurian time and collided with the Eurasian plate in Triassic (Alavi 1991). During Mesozoic extensional phases, upper Triassic rift volcanism and plutonism, and deposition of shaly, coal-bearing Shemshak Formation occurred (Berberian 1983). Finally, the Central Alborz zone was developed during Upper Jurassic and Lower Cretaceous times with shallow marine limestone, and alkaline basalt eruptions (Aghanabati 2004). Volcanic activity in this zone started in Eocene and lasted till Tertiary as evidenced by fault-related thermal activities and occurrence of hot springs in parts of the zone including the Ramsar area (Torbehbar and Liseroudi 2015). The outcropping geological formations, in a decreasing order of age are Kahar shale and Soltanieh dolomite (Precamberian), Baruat sandstone (Camberian), Mila dolomite, limestone and sandstone (Camberian-Ordovisian), Ordovician shale, Mobarak limestone and shale (Carbonifer), Dorud sandstone, Ruteh limestone and Nesen chert limestone (Permian), Elika dolomite and Shemshak shale (Triassic), Lar limestone (Jurassic), Tiz kuh limestone (Jurassic-Cretaceous), Chalus limestone (Cretaceous), Karaj limestone, tuff and gypsum and Upper red mudstone (Tertiary), Marine deposites (Quaternary), and Recent alluvium (Alavi 1991). Also, granodioritic, granitoid, luecogranitic, and quartzmonzonitic intrusive bodies are common in the area, with lithostratigraphic age of Paleocene and Oligocene (Fig. 1) (Doroozi et al. 2016).

Field relations and sampling

A total of 20 spring water samples were collected from 20 different springs in August 2017. The samples were collected from the most popular springs in the area discharging from different lithological formations. Six samples including S3, S4, S5, S6, S7, and S8 are located South of the Ramsar city (Ramsar's springs), and the rest are scattered in rural areas. The characteristics of the sampling stations are presented in Table 1. Physicochemical parameters such as temperature, pH, and oxidation-reduction potential (ORP) were measured in situ, using a waterproof Eutech portable meter (model PCD 650). ORP was measured using Ag/AgCl electrode and converted to standard hydrogen potential (Eh) by correcting for the electrode potential of the reference electrode (Muñoz et al. 2015). Each sample was collected in a separate polyethylene bottle for measuring selected cations and anions, as well as PTEs and radioactive elements. The containers were first pre-washed with dilute hydrochloric acid and then rinsed with distilled water.

Sample analysis

In order to measure the major and minor ions, samples were placed into pre-washed 1-L polyethylene bottles. The bottles were first rinsed with spring water and then completely filled and tightly closed with caps and kept at 4 °C. Within 2 weeks from the collection date, the samples were analyzed at the

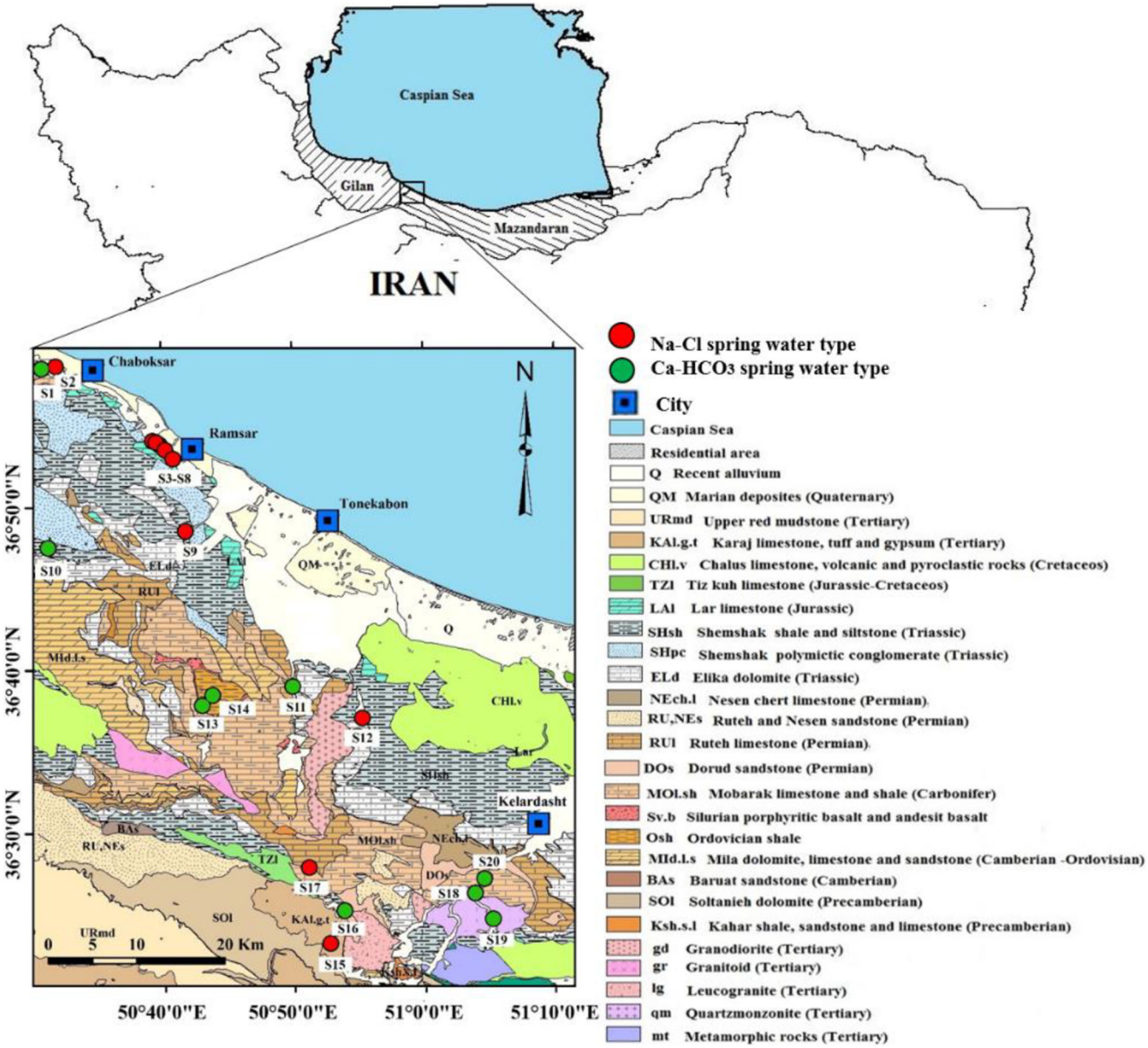

Fig 1 General geological formations and spatial distribution of sampling stations in the study area

Hydrochemical Laboratory of the Department of Earth Sciences, Shiraz University, Iran. Total dissolved solid (TDS) load was determined by evaporation method. Bicarbonate (HCO_3^-) and chloride (Cl^-) were quantified by acid and $AgNO_3$ titration method, respectively. Also, calcium (Ca^{2+}) and magnesium (Mg^{2+}) were measured using titration with EDTA. Sodium (Na^+) and potassium (K^+) were analyzed using a flame photometer (PFP7, Jenway). Sulfate (SO_4^{2-}) was determined by spectrophotometry (DR/2500, Hach, USA) (APHA 1995). The accuracy of the major ions analyses was checked by computing the cation-anion charge balance. The ionic balance error for the studied ions was within ± 5%.

To analyze PTEs, samples were filtered using 0.45 μm syringe filters to remove suspended solids and then stored in pre-washed 60-mL plastic bottles before analysis. Afterwards, they were acidified (pH < 2) using ultrapure nitric acid to prevent adsorption on containers and avoid the growth of microorganisms (El-Mageed et al. 2013). All samples were stored at 4 °C and then sent to the laboratory. The concentrations of Al, As, Cd, Cr, Cu, Fe, Hg, Mn, Mo, Ni, Pb, Sb, and Zn were measured using inductively coupled plasma mass spectrometry (ICP-MS) in Activation Laboratories Ltd. Ontario, Canada. The QA/QC process for PTEs was carried out using analytical duplicates/replicates, blank reagents, and certified reference material (IV-STOCK-1643). Average recoveries were in the range of 95–110%, depending on the element, while the precision, as the relative standard deviation, was less than 6%. The detection limits were below, 0.01 μg/L for Cd, Pb, and Sb, 0.03 μg/L for

Table 1 Description of studied springs water in the study area

Sample	Name	Main use	Latitude	Longitude
S1	Damkesh	Drinking, bathing	36° 58′ 33.41″	50° 30′ 56.06″"
S2	Ab Torsh	Dermal diseases treatment	36° 58′ 41.95″"	50° 32′ 00.81″
S3	Ab Siah	Balneology	36° 53′ 55.70″	50° 39′ 57.13″
S4	Hotel 1	Balneology	36° 54′ 09.73″	50° 39′ 25.67″
S5	Zir Pol	Balneology	36° 54′ 05.07″	50° 39′ 42.18″
S6	Hotel 2	Balneology	36° 54′ 05.10″	50° 39′ 41.29″
S7	Talesh Mahaleh	Without use	36° 53′ 36.40″	50° 40′ 23.27″
S8	Khak Sefid	Without use	36° 53′ 04.21″"	50° 40′ 59.44″
S9	Jolo	Agriculture	36° 48′ 38.02″	50° 41′ 57.57″
S10	Emam Zadeh	Rheumatism treatment	36° 47′ 33.21″	50° 31′ 30.89″
S11	Yandasht	Drinking, bathing	36° 39′ 08.00″	50° 50′ 09.61″
S12	Falak Deh	Balneology	36° 37′ 11.94″	50° 55′ 27.95″
S13	Asal Mahaleh	Drinking, bathing	36° 37′ 56.32″	50° 43′ 17.91″
S14	Barseh	Drinking, bathing	36° 38′ 33.94″	50° 44′ 04.65″
S15	Shelef Darjan	Balneology	36° 23′ 20.27″	50° 53′ 05.78″
S16	Ab Madan Maran	Kidney stone treatment	36° 25′ 21.55″	50° 54′ 09.21″
S17	Yuag	Dermal diseases treatment	36° 28′ 00.06″	50° 51′ 26.76″
S18	Pir Zan	Dermal diseases treatment	36° 26′ 26.08″	51° 04′ 02.65″
S19	Lat Kamar	Without use	36° 24′ 51.16″	51° 05′ 24.88″
S20	Zar Nama Sang	Drinking, Bathing	36° 27′ 20.25″	51° 04′ 45.00″

As, 0.10 μg/L for Mn and Mo, 0.20 μg/L for Hg and Cu, 0.30 μg/L for Ni, 0.50 μg/L for Zn and Cr, 2 μg/L for Al, and 10 μg/L for Fe. Water samples for radioactive elements analysis were filtered using a 0.45 μm vacuum pump and stored in pre-washed 1-L polyethylene Marinelli beakers and were acidified (pH < 2) using ultrapure nitric acid. The Marinelli beakers were then sealed for 30 days to reach the secular equilibrium before radiometric analysis at 4 °C. The concentrations of ^{226}Ra, ^{232}Th, and ^{40}K were measured using gamma spectroscopy with p-type coaxial high-purity germanium detector with a relative efficiency of 40% and resolution of 1.90 keV for the 1332.5 keV gamma ray emission of Co-60 in Shiraz University Radiation Research Center.

Energy calibrations were performed using calibration point sources (^{241}Am, ^{133}Ba, ^{137}Cs, and ^{60} Co). The efficiency calibration of the gamma spectrometer was done by using multinuclides standard solution produced by the International Atomic Energy Agency (IAEA). Standard samples of the Atomic Energy Organization of Iran (AEOI) were used for quality assurance. A Marinelli beaker filled with distilled water was applied to strip the background radioactivity away from the samples. The spectrum of each sample was collected for 72 h. Determination of ^{40}K was directly carried out by its emission energy of 1460.7 keV. The activity of ^{226}Ra was determined based on gamma ray energies of 295.22 and 351.93 keV (from ^{214}Pb) and 609.31, 1120.29, and 1764.49 keV (from ^{214}Bi). Furthermore, the activity concentration of ^{232}Th was determined based on gamma ray energies of 338.32 and 911.20 keV (from ^{228}Ac), and 583.19 keV (from ^{208}Tl) (Ahmad et al. 2019; Arafat et al. 2017; Al-Shboul et al. 2017). The minimum detectable activity of the system for ^{226}Ra, ^{232}Th, and ^{40}K was 0.30, 0.15, and 2.50 Bq/L, respectively (ASTM 2004).

Statistical analysis

Statistical analysis and mathematical calculations were carried out using IBM-SPSS Statistics V. (21). All non-detected (ND) concentrations were assumed to be equal to 75% of the detection limit. Data distribution was checked with the Shapiro-Wilk test. Also, to understand the inter-elemental relationships of analyzed variables, correlation matrix analysis and principal component analysis (PCA) were carried out. The geological and spatial variation maps were also developed using Arc Map V. (10.3).

Human health risk assessment

Human health risk evaluation was applied to determine the potential detrimental effects of the chemicals found in the tested samples considering USEPA and ICRP risk assessment methodologies. In this study, health hazards of ingestion and dermal absorption pathways for PTEs and radioactive elements were estimated for children and adults.

Exposure assessment of PTEs

The chronic daily intake (CDI $_{Ingestion}$ and CDI $_{Dermal}$), hazard quotient (HQ) and hazard index (HI) were estimated based on USEPA standards. CDI represents daily exposure of the population to PTEs in μg/L/day. The values of CDI were calculated using the following equations (USEPA 2004):

$$\text{CDI Ingestion} = \frac{C_X \times \text{IngR} \times \text{EF} \times \text{ED}}{\text{BW} \times \text{AT}} \quad (1)$$

$$\text{CDI Dermal} = \frac{C_X \times \text{SA} \times \text{AF} \times \text{ABS}_d \times \text{ET} \times \text{EF} \times \text{ED} \times \text{CF}}{\text{BW} \times \text{AT}} \quad (2)$$

where C_X is the concentration of element (x); IngR represents ingestion rate; EF is exposure frequency; ED is exposure duration; BW is body weight; AT is average time; SA is exposure skin area; AF is adherence factor; ABS_d is dermal absorption fraction; ET is exposure time; and CF is unit conversion factor. In this study, it was assumed that the consumers receive water, in accordance with USEPA standards, listed in Table S1.

Non-carcinogenic risk of PTEs

Hazard quotient (HQ) was calculated to determine the potential non carcinogenic human health risk posed by exposure to PTEs. It was determined through a quotient between CDI and reference dose (RfD) using the following equations (USEPA 2004):

$$\text{HQ Ingestion} = \frac{\text{CDI}_{\text{Ingestion}}}{\text{RfD}_{\text{Ingestion}}}; \text{HQ Dermal} = \frac{\text{CDI}_{\text{Dermal}}}{\text{RfD}_{\text{Dermal}}} \quad (3)$$

The RfD used to characterize HQ values for both groups of population was obtained in μg/L/day unit from USEPA (2010) and WHO (2017) (Table S4 and S5). To assess the health risk of a combination of PTEs, the individual HQs was summed up to form hazard index (HI). The HI were obtained from the following equation (USEPA 2004):

$$\text{HI} = \sum_{x=1}^{n} \text{HQ}_X \quad (4)$$

If HQ and HI exceed 1, there is an unacceptable risk of adverse non-carcinogenic effects on health, while HQ < 1 is an acceptable level of risk.

Carcinogenic risk of PTEs

Carcinogenic risk (CR) was calculated to evaluate the probability of an individual developing cancer over a lifetime as a result of exposure to a PTE using CDI multiplied by the slope factor (SF), based on the following equations (USEPA 2014):

$$\text{CR} = \text{CDI}\ (\mu\text{g/L/day}) / \text{SF}\ (\mu\text{g/L/day}) \quad (5)$$

According to the regulated threshold from USEPA guidance, the carcinogenic risks would occur when the risk values exceed 1.0E-04 (USEPA 2014). The $SF_{Ingestion}$ values for As, Cd, Cr, and Pb are 1.5E+03, 6.1E+06, 5.0E+05, and 8.5E+03, respectively. Moreover, the SF $_{Dermal}$ for As is 3.66E+03. The CR values for other PTEs were not calculated due to unavailability of the SF values (USEPA 2014).

Exposure assessment of radioactive elements

In order to assess the human health risk of radiation, annual effective dose (DR_w) in terms of ingestion of radionuclides was calculated for children and adults, using the following equation (USEPA 2014; ICRP 1996):

$$\text{DR}_W = \text{A}_W \times \text{IR}_W \times \text{ID}_F \quad (6)$$

where DR_W is annual effective dose (mSv/year); A_W is activity concentration of radionuclide in water sample (Bq/L); IR_W is ingestion rate for a person in one year; and ID_F is effective dose equivalent conversion factor (mSv/Bq) as shown in Table S8. Doses were computed by considering a consumption rate 350 and 730 L/year for children and adults, respectively (WHO 2011). Also, external hazard index (H_{ex}) is used to assess dermal radiological hazard due to emitted gamma ray of each sample used for bathing and balneology, using the following equation (UNSCEAR 2000):

$$\text{H}_{ex} = (\text{A}_{Ra}/370) + (\text{A}_{Th}/259) + (\text{A}_K/4810) \leq 1 \quad (7)$$

The values must be less than unity (< 1) for the radiation hazard to be negligible.

Lifetime risk of radioactive elements

Cancer and hereditary risks due to low dose known as lifetime risk were estimated using the ICRP cancer risk methodology according to the following equations (ICRP 2012):

$$\text{Radiation Cancer Risk} = \text{DR}_W \times \text{DL} \times \text{RF}_{\text{Cancer risk}} \quad (8)$$

$$\text{Radiation Hereditary Effects} = \text{DR}_W \times \text{DL} \times \text{RF}_{\text{Hereditary effects}} \quad (9)$$

where DR_W is annual effective dose (Sv/year); DL is duration of life (70 years); and RF is risk factor (1/Sv). Risk factors for cancer risk and hereditary effects are 5.5E-02 and 2.0E-03, respectively. Similar to the regulated threshold of PTEs, the carcinogenic and hereditary effects of radioactive elements would occur when the risk values exceed 1.0E-04 (ICRP 2012).

Results and discussion

Spring water physicochemical characteristics

Statistical description of physicochemical characteristics is presented in Table 2. According to the piper diagram (Fig. S1), water samples in the study area are of two Na-Cl and Ca-HCO_3 types (Piper 1953). The temperature ranged from 24 to 48 °C with a median of 32.40 °C for Na-Cl type and 10.5 to 16 °C with a median of 13.5 °C for Ca-HCO_3 type. Based on water temperature grouping (Meinzer 1965), all Na-Cl type springs must be classified as thermal springs ($T > 21$ °C) while Ca-HCO_3 type springs proved to be non-thermal springs ($T < 21$ °C). pH ranged from 6.10 to 7.24 with a median of 6.58 for Na-Cl type and 6.18 to 9.15 with a median of 7.76 for Ca-HCO_3 type. Eh ranged from 9 to 367 mV with a median of 89 mV for Na-Cl type and 279 to 321 mV with a median of 301 mV for Ca-HCO_3 type. TDS varied from 0.420 to 103 g/L with a median of 15.7 g/L for Na-Cl type and 0.110 to 0.850 g/L with a median of 0.220 g/L for Ca-HCO_3 type. Water type in all potable springs was Ca-HCO_3 type with hydrochemical properties being within the recommended water quality standards set by WHO (WHO 2017).

PTEs distribution

Statistical description of selected elements concentrations in spring water samples is shown in Table 2. The median

Table 2 Statistical summary of physicochemical characteristics, ion concentrations (mg/L), PTEs concentrations (μg/L), and radioactive element concentrations (Bq/L) for spring water samples ($n = 20$)

Parameter	Range Na-Cl type ($n = 11$)	Mean ± SD	Median	Range Ca-HCO_3 type ($n = 9$)	Mean ± SD	Median	Standard permissible value[a]
T (°C)	24–48	32 ± 7.98	32.40	10.5–16	13 ± 1.76	13.5	
Eh (mV)	9–367	172 ± 150	89	279–321	302 ± 16	301	
pH	6.10–7.24	6.67 ± 0.380	6.58	6.18–9.15	7.83 ± 0.810	7.76	6.5–8.5
TDS (g/L)	0.420–103	28.90 ± 38.2	15.7	0.110–0.850	0.310 ± 2.34	0.220	1
HCO_3^-	9.15	1067.67 ± 337	762	91.5–1220	375 ± 390	183	-
Cl^-	377–70,840	17,921 ± 25,965	8855	5.31–230	40.2 ± 74.2	8.85	200
SO_4^{2-}	2.40–288	118.25 ± 99.9	84	2.40–108	15.5 ± 34.7	3.36	200
Ca^{2+}	22.0–4500	1170 ± 1456	806	22–320	107 ± 115	55	75
Mg^{2+}	18.3–660	200.90 ± 198	120	3–72	17.4 ± 21.6	12	< 30 if SO_4^{2-} is 250, > 150 if SO_4^{2-} is less than 250
Na^+	133–42,880	10,785 ± 15,533	5101	1.14–137	31.2 ± 50.1	3.67	200
K^+	313–1.95	78.53 ± 94.2	42.9	0.390–7.02	2.55 ± 2.03	1.56	120[b]
Al	12–27	8.90 ± 9.27	1.50	7–51	17.5 ± 14.4	16.0	200
As	0.150–164	17.82 ± 48.6	1.53	0.070–476	53.3 ± 158	0.440	10
Cd	0.010–0.120	0.020 ± 0.034	0.007	0.010–0.100	0.021 ± 0.030	0.010	3
Cr	1.20–2.80	1.050 ± 0.872	0.375	0.800–3.40	1.80 ± 1.019	1.50	50
Cu	1–2.10	0.818 ± 0.810	0.150	0.900–1.70	1.08 ± 0.450	1.00	3000
Fe	40–90	32.273 ± 30.9	7.50	20–10,400	1245 ± 3437	40	300
Hg	42–212	23.222 ± 63.8	0.150	ND	-	-	1
Mn	21.5–506	153.818 ± 178	58.7	0.700–1460	164 ± 485	1.30	100
Mo	0.500–3.30	0.602 ± 0.993	0.075	0.500–7.200	2.31 ± 2.23	1.40	10
Ni	0.500–1.10	0.531 ± 0.387	0.225	0.300–1.500	0.780 ± 0.436	0.800	70
Pb	0.430–10.1	2.79 ± 3.76	0.680	0.530–1.91	0.780 ± 0.436	0.800	10
Sb	1.72–3.06	1.009 ± 1.12	0.075	1.78–4.66	2.69 ± 0.856	2.58	20
Zn	6.90–16	5.37 ± 6.25	0.375	5.90–15.5	10.1 ± 3.40	8.20	4000
^{226}Ra	0.70–65	13 ± 24	1.5	0.30–0.45	0.28 ± 0.08	0.22	1
^{232}Th	0.16–4	0.90 ± 1.4	0.16	ND	-	-	1
^{40}K	2.6–9.5	3 ± 2.4	1.9	ND	-	-	10[c]

ND, non-detected; *SD*, standard deviation

[a] WHO (1984, 2017)

[b] Tirkey et al. (2017)

[c] ICRP (1990)

concentrations of PTEs (μg/L) recorded among all Na-Cl type springs were as follows: Mn > Fe > Hg > As> Zn > Al > Pb > Cr > Sb > Cu > Mo > Ni > Cd and for Ca-HCO_3 type were Fe > Mn > As> Al > Zn > Sb > Mo > Cr > Cu > Ni > Pb > Cd > Hg. In order to envisage the distribution of PTEs, their concentration was compared with permissible levels recommended for potable water (WHO 2017). The results showed that the concentrations of Al, Cd, Cr, Cu, Pb, Mo, Ni, Sb, and Zn were well below the permissible level (Table 2). On the contrary, the concentration of Fe, Mn, As, and Hg in some stations was above the recommended permissible level (Fig. 2).

Iron concentration in Na-Cl type ranged from 40 to 90 μg/L with a median of 7.50 μg/L and in Ca-HCO_3 type ranged from 20 to 10,400 μg/L with a median of 40 μg/L. In thermal fluids, Fe is commonly mobilized by a variety of metal-ligand complexes such as OH^-, HCO_3^-, and Cl^- (Robb 2004). According to Brookins (2012), Eh-pH diagrams at 25 °C and 1 bar pressure, the dominant Fe species are solid $Fe(OH)_3$ and Fe_2O_3 (Fig. S2a, S2b). Hence, rust-colored carbonate sediments surround the springs with elevated Fe content including S15, S16, S17, and S20. Concentrations higher than permissible level (300 μg/L) were measured in Ab Madan Maran (S16) (10,400 μg/L) and Zar Nama Sang (S20) (580 μg/L) (Fig. 2a). Since both these springs are Ca-HCO3 type, it can be said that high concentrations of Fe are the result of iron-rich carbonate dissolution or mixing with Fe-rich thermal fluids. Iron is essential for human health, but it is heavily toxic in high concentration and causes cardiovascular, central nervous system diseases along with nephrotic and hepatic problems (Goldhaber 2003). Despite the toxic effects of Fe on the kidneys, locals believe that Ab Madan Maran (S16) spring water is beneficial for kidney stone treatment. Moreover, the Zar Nama Sang (S20) spring water in the study area is mainly used for drinking and hence may lead to widespread Fe toxicity in the study area.

Manganese concentration in Na-Cl type water ranged from 21.5 to 506 μg/L with a median of 58.7 μg/L and in Ca-HCO_3 type ranged from 0.700 to 1460 μg/L with a median of 1.30 μg/L. The concentration in Na-Cl type was significantly higher than Ca-HCO_3 type. Figure S2c shows that Mn forms soluble (Mn^{2+}) species in Mn-C-O-S-H system (Brookins 2012). Furthermore, Mn is highly mobile in saline water due to complexing with Cl^- (Robb 2004). The high concentration of Mn is believed to cause mental diseases including Alzheimer and manganism (ATSDR 2007). Manganese content in Ab Siah (S3) (506 μg/L), Talesh Mahaleh (S7) (407 μg/L), Khak Sefid (S8) (127 μg/L), Shelef Darjan (S15) (354 μg/L), Ab Madan Maran (S16) (1460 μg/L), and Yuag (S17) (115 μg/L) were higher than permissible limit (100 μg/L) (Fig. 2b).

Arsenic may cause serious chronic human toxicity like arsenicosis, hyperkeratosis, and melanosis and affect the nervous system, skin, and the cardiovascular system (Huq et al. 2019; Rahman et al. 2009). In the present study, As varied from 0.150 to 164 μg/L with a median of 1.53 μg/L in Na-Cl type and 0.070 to 476 μg/L with a median of 0.440 μg/L in Ca-HCO_3 type spring water. In thermal fluids, arsenate ion (As^{5+}) aqueous complexes are stable at higher pH values (Robb 2004). Hence, in almost all studied spring water, the measured As content must be arsenate ($H_2AsO_4^-$ and $HAsO_4^{2-}$) (Brookins 2012) (Fig. S2d, S2e). Arsenic content was significantly high in Shelef Darjan (S15) (164 μg/L), Ab Madan Maran (S16) (476 μg/L), and Yuag (S17) (591 μg/L) compared with water quality standard (10 μg/L) (Fig. 2c). Mercury was detected in Talesh Mahaleh (S7) (212 μg/L) and Khak Sefid (S8) (42 μg/L) springs. These values are approximately 200 times the standard limit (1 μg/L) for S7 and 40 times for S8 (Fig. 2d). As shown in Fig. S2f, Hg^0 has a wide stability field in aqueous systems (Brookins 2012). The origin of high natural Hg concentrations is, in fact, restricted to thermal systems (Gustin et al. 2008; Simbahan et al. 2005) were it can be transported either as a vapor or elemental Hg (Robb 2004). These two springs are located in agricultural areas, therefore, there is a high potential of soil contamination due to uncontrolled runoffs. Hence, symptoms such as lung injury, hypertension, renal dysfunction, and neurological disorders (Jan et al. 2015) may be observed due to Hg toxicity.

Radioactive elements distribution

Statistical description of activity concentrations of ^{226}Ra, ^{232}Th, and ^{40}K, in the study area, is summarized in Table 2. The median concentrations were $^{226}Ra > {}^{40}K > {}^{232}Th$. All these radionuclides are classified as group 1 human carcinogens (Gbadago et al. 2011; ICRP 1996), because they accumulate and decay in the body and, ultimately, cause significant exposure of the surrounding tissues to radiation (Iyengar 1990). ^{226}Ra concentration in Na-Cl type springs water ranged from 0.70 to 65 Bq/L with a median of 1.5 Bq/L and in Ca-HCO_3 type ranged from 0.30 to 0.45 Bq/L with a median of 0.22 Bq/L. Maximum ^{226}Ra was measured in Ramsar's springs (S3, S4, S5, S6, S7, and S8) (Fig. 3a). Seemingly, these springs distributed ^{226}Ra in populated rural and agricultural areas of Ramsar city. In an aqueous system, Ra occurs only in the divalent state (Ra^{2+}) and behaves like other alkaline earth elements. Hence, adsorption to active surfaces and co-precipitation with other elements are two primary factors that control ^{226}Ra concentration in water (Molinari and Snodgrass 1990). As it can be seen in Fig. S2g, $RaSO_4$ is the dominant solid species of Ra in Ra-O-H-C-S system (Brookins 2012). Therefore, its elevated concentration was expected in spring sediment. Unlike ^{226}Ra, ^{232}Th and ^{40}K were below the detection limit in most of the studied springs (Fig. 3b,c). ^{40}K was detected only in three Na-Cl type springs including Ab Siah (S3), Khak Sefid (S5), and Talesh Mahaleh (S7). In Cl-rich thermal fluids, K may be removed from the

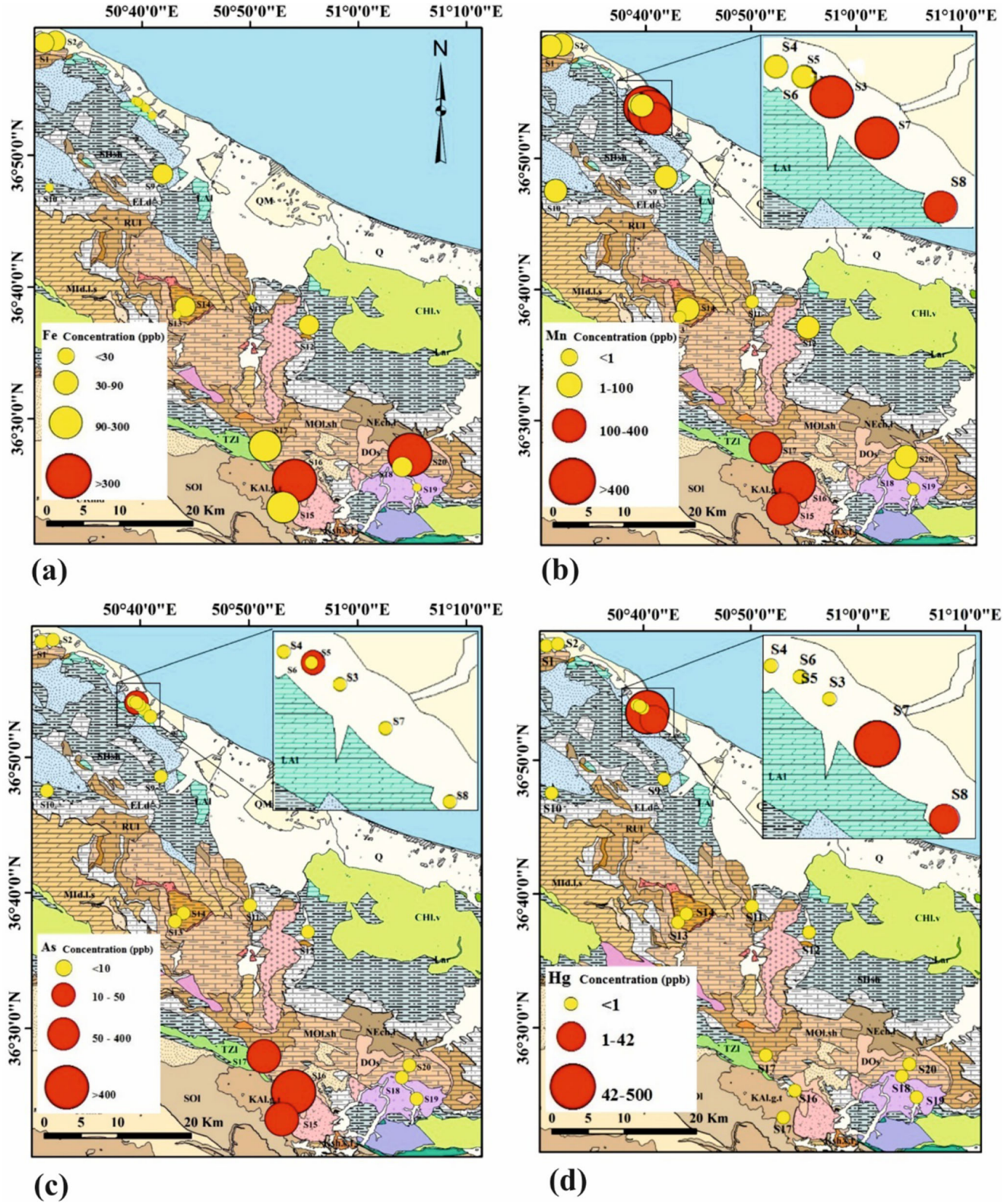

Fig 2 Spatial distributions of PTEs in the study area. **a** Fe, **b** Mn, **c** As, and **d** Hg (red circles represent concentrations above the recommended permissible limit for drinking water)

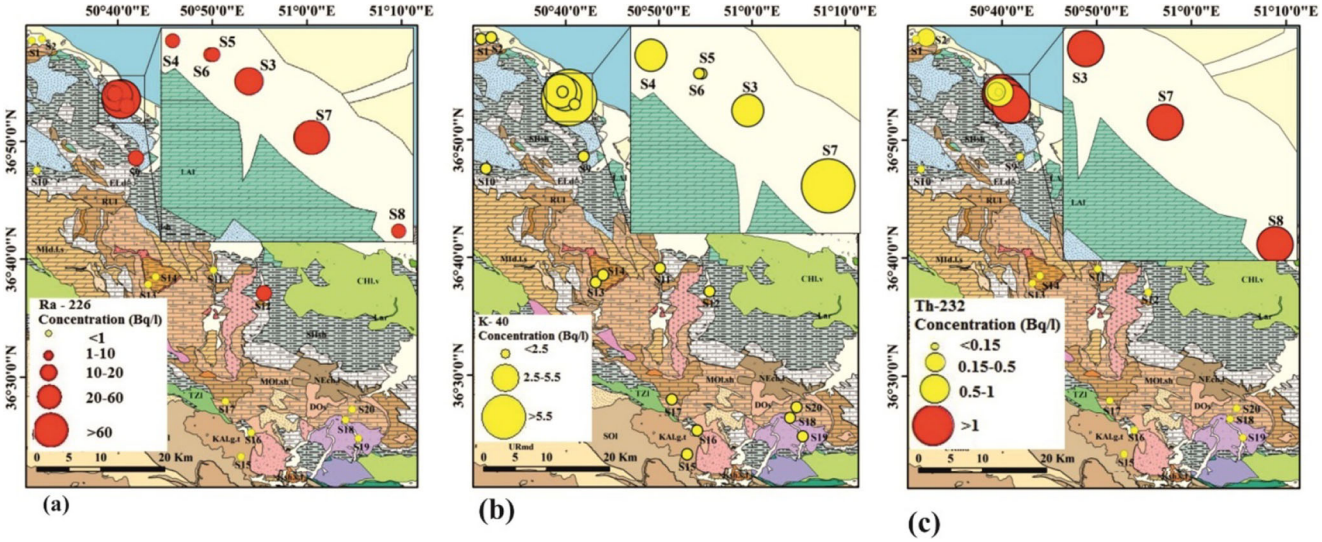

Fig 3 Spatial distributions of radioactive elements in the study area. **a** ^{226}Ra, **b** ^{40}K, and **c** ^{232}Th (red circles represent concentrations above the recommended permissible limit for drinking water)

aqueous phase by the conversion of clay minerals (for instance, the conversion of montmorillonite in to illite and chlorite) (Nicholson 1993; Merian 2004), and hence may be concentrated in underground clay layers.

Also, ^{232}Th was not detected in Ca-HCO_3 type. The value of ^{232}Th varied from 0.16 to 4 Bq/L with a median of 0.16 Bq/L in Na-Cl type. Its concentration in S3 (4.05 Bq/L), S7 (3.15 Bq/L), and S8 (1.16 Bq/L) was higher than permissible limit (1 Bq/L) (Fig. 3c). The dominated species in Th-S-O-H system at 25 °C and 1 bar pressure is solid ThO_2 (Fig. S2h) (Brookins 2012). In fact, Th is undetectable in spring water even near the ore bodies because of the low solubility of its host minerals. Furthermore, dissolved Th has a tendency to be adsorbed onto clay-sized particles in aquifers and precipitate (Ahmad et al. 2019; Gbadago et al. 2011; Labidi et al. 2010). However, Th solubility in thermal water with pH < 8 is higher than non-thermal water due to the presence of ligands such as F^-, SO_4^{2-}, and PO_4^{2-} (Langmuir and Herman 1980). As shown in Figs. 2 and 3, the distribution of PTEs (As, Fe, Hg, and Mn) and radioactive elements (^{226}Ra, ^{40}K, and ^{232}Th) in thermal Na-Cl type springs follows a general pattern. That is high concentrations of As and Fe occur in south while Hg, ^{226}Ra, ^{40}K, and ^{232}Th occur in north of the study area. However, Mn showed a nearly uniform distribution pattern in all Na-Cl type springs.

Correlation analysis

The Shapiro-Wilk test was applied to evaluate the normality of the variables, describing springs water characteristics. The results indicated that the distribution of variables is non-normal. Thus, Spearman's correlation analysis was utilized to determine the associations. The correlation matrix of the analyzed parameters is presented in Table S2. A significant positive correlation between As and Fe ($P < 0.05$, $r = 0.54$) suggests a common source (Aboyeji and Eigbokhan 2016). Radioactive elements displayed a significant positive correlation with Mn ($P < 0.01$, $r > 0.60$) and a significant negative correlation with pH and Eh ($P < 0.01$, $r < -0.6$) (Ahmad et al. 2019). Therefore, the high concentrations of radioactive elements were measured in acidic and reduced springs water. Apart from common origin, such a condition prohibits formation of Mn-oxyhydroxides resulting in reduced adsorption of radioactive elements (Moore and Reid 1973). Moreover, elevated Eh and pH (> 8) are required for oxidation of soluble Mn (Mn^{2+}) to insoluble form (Mn^{4+}) (Hallberg and Johnson 2005). Since there is a positive correlation between radioactive elements and Hg ($P < 0.05$, $r > 0.5$), it follows that these elements probably originated from a common source. Radium shows a strong positive correlation with all analyzed cations and anions ($P < 0.01$, $r > 0.7$), except for SO_4^{2-} and HCO_3^-. Therefore, it may be concluded that these anions play no role in ^{226}Ra mobility in thermal fluids (Shabana and Kinsara 2014). Furthermore, radium exists in water only in Ra^{2+} form and during co-precipitation process in the presence of SO_4^{2-}, and HCO_3^- forms insoluble radium-barium sulfate and radium-calcium carbonate (Stackelberg et al. 2018). Thus, the concentration of ^{226}Ra decreases in water with increasing SO_4^{2-} and HCO_3^-. A significant positive correlation exists between TDS and radioactive elements, Mn, and Hg. The reason is probably the fact that high TDS in thermal fluids increases desorption of metals from adsorbents in the process of competitive exchange with other cations generally known as competing ion effect (Moore and Shaw 1998 ; Sherif and Sturchio 2018). Finally, a positive inter-relationship was observed between temperature and a group of parameters

including, radioactive elements, Mn, and Hg, confirming a high temperature interaction between rock and spring water (Roba et al. 2012).

Principal component analysis (PCA) of PTEs and radioactive elements

The suitability of the data for PCA was examined using Kaiser-Meyer-Olkin (KMO) and Bartlett's sphericity tests. The results of the Kaiser-Meyer-Olkin (0.57) and Bartlett's test ($P < 0.001$) confirmed the suitability of variables for PCA. The PCA results of various physicochemical parameters and of elements are summarized in Table S3. Three components were extracted explaining 88.26% of the total variance using factor extraction with an eigenvalue > 1 after Varimax rotation with Kaiser Normalization. The PC1 constituted 58.44% of the total variance, showing positive loadings for TDS, radioactive elements, and Mn, Hg, Cl^-, Ca^{2+}, Mg^{2+}, Na^+ and K^+. However, it displayed negative loadings for Eh and pH. Therefore, PC1 justifies the high concentrations of the components in thermal Na-Cl type springs (Ramsar's springs). PC1 also suggested a common origin and/or hydrochemical behavior for these parameters. PC2 formed 17.85% of the total variance demonstrating positive loadings for SO_4^{2-}, HCO_3^-, and temperature, and a negative loading for pH. PC2 shows higher H^+ release due to breaking up of water molecules at high temperature (Holman et al. 2012) and dissolution of magmatic-derived CO_2 (Bagnato et al. 2009) and H_2S (Nicholson 1993) both responsible for the acidification of spring water. PC3 indicated that 11.97% of the total variance is dominated by As, Fe, Mn, while HCO_3^- demonstrated the role of HCO_3^- ion as a ligand in the transmission of elements in thermal systems.

Potential risk assessment for human health

In the study area, no remarkable relationship was found between the measured characteristics of Ab Torsh (S2), Ab Madan Maran (S16), Yuag (S17), and Pir Zan (S18) spring water and their use by locals for renal stone and dermal diseases treatment (Table 1). Due to high toxicity of PTEs and radioactive elements, human health risk assessment was carried out for children and adults. As presented in Table 1, these evaluations are limited to some Na-Cl and Ca-HCO_3 springs used for drinking and bathing/balneological purposes.

Human risk assessment of PTEs

PTEs concentrations in spring water were used to assess human exposure through ingestion and dermal contact. All results for PTEs health risk assessment for children were above those for adults (Table S4, S5, and S6). However, one must bear in mind that similar concentrations of the same PTE in an environment can pose various health complications to different population groups due to differences in physiology and exposure patterns (Singh et al. 2018); for instance, detoxification mechanisms are undeveloped in children. Moreover, the proportion of skin surface area to body mass, and also water consumption rate are two important factors while dermal and ingestion exposures are higher in children compared with adults (USEPA 2011).

The results showed that $CDI_{Ingestion}$ were more than CDI_{Dermal} for all PTEs. Therefore, ingestion is the dominant exposure rout in the study area. The $CDI_{Ingestion}$ and CDI_{Dermal} of Ca-HCO_3 type water showed that both groups of population consumed and absorbed PTEs in the following order: Fe > Al > Zn > Sb > Cr > Mo = Mn > Cu > Ni > Pb > As > Cd. Therefore, Fe was found to be the highest consumed element through ingestion and dermal contact in Ca-HCO_3 type water (Fig. 4, Table S4, S5). Furthermore, the result of $HQ_{Ingestion}$ and HQ_{Dermal} for this water type showed that both groups of population are exposed to PTEs in the following order: Sb > As > Cr > Pb > Fe > Mo > Mn > Cd > Ni > Zn > Cu > Al, where Sb is the consumed element with the highest mean $HQ_{Ingestion}$ and HQ_{Dermal}. Among the Ca-HCO_3 type springs, the higher values of HQ were observed in Zar Nama Sang (S20) in both population groups (Table S4, S5). However, HQ was found to be < 1 in all stations, which indicates that Ca-HCO_3 type water used by locals is safe for human health.

The CDI_{Dermal} analysis of spring water with Na-Cl type showed that in both groups of population, the order of absorbed elements is Mn > As > Fe > Al > Pb > Zn > Cr > Mo > Sb > Cu > Ni through dermal absorption. Mn dermal absorption rate was high compared with other elements. Furthermore, the results of HQ_{Dermal} for spring water revealed that both groups absorbed elements in the following order: As > Mn > Sb > Cr > Pb > Cd > Fe > Mo > Ni > Al > Zn > Cu, where the element with the highest mean is As. The higher HQ_{Dermal} occurs at Shelef Darjan (S15) in both groups (Fig. 4b and Table S6). The obtained HQ_{Dermal} for Na-Cl type was lower than one (< 1) in all sites, indicating that this type of water is also suitable for bathing and balneological purposes. Nevertheless, the HQ_{Dermal} values of As, Mn, and Pb in Na-Cl type were approximately 50, 100, and 5 times higher than those in Ca-HCO_3 type. Hazard index (HI) for PTEs was also calculated to investigate the rate of ingestion and dermal absorption. $HI_{Ingestion}$ and HI_{Dermal} for all elements are lower than the desirable limit (< 1) suggesting low health risk for both population groups (Table S7).

The mean carcinogenic risk through ingestion of Ca-HCO_3 type water varied as As > Pb > Cr > Cd, depending upon the distribution of the element's concentrations. The highest cancer risk of ingestion for As was observed in Yandasht (S11) (Table S4). Also, cancer risk of As through dermal contact of Na-Cl type was more than

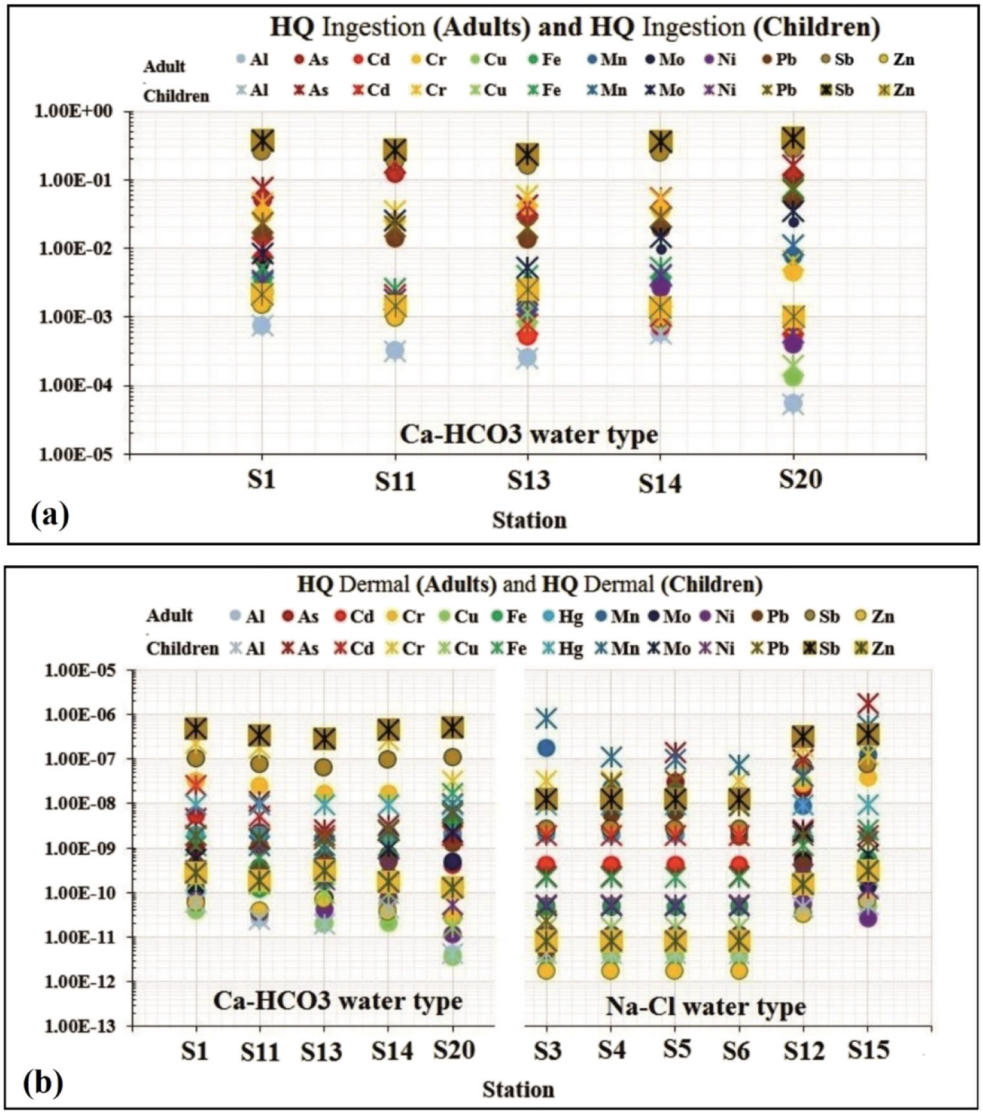

Fig 4 Distribution of hazard quotient (HQ) for **a** ingestion and **b** dermal contact in children and adults along the sampling stations

100 times higher than Ca-HCO_3 type. Nevertheless, the cancer risk through ingestion and dermal exposure of spring water, for both groups, were less than admissible levels (1.0E-04).

Human health risk assessment of radioactive elements

The annual effective dose associated with radiation exposure through ingestion of Ca-HCO_3 type spring water was estimated for adults and children. The annual effective dose varied generally in the order $^{226}Ra > {}^{232}Th > {}^{40}K$ for both groups of population. The doses absorbed by children were higher than adults. The mean total annual effective doses received by adults and children were 8.94E-02 mSv/year and 1.05E-01 mSv/year, respectively. The highest total DR_w was found in Yandasht (S11) (1.19E-01 mSv/year for adults and 1.46E-01 mSv/year for children) (Fig. 5, Table S8). Based on UNSCEAR's (2013) recommended reference levels of total effective doses during 1-year consumption of drinking water (1.00E-01 mSv/year for adults, and 2.00E-01 mSv/year for children), the doses of Yandasht (S11) spring water were slightly above the recommended dose for adults.

The calculated external hazard index for Na-Cl type (2.71E-03 to 1.77E-01) is higher than Ca-HCO_3 type (1.43E-03 to 2.04E-03). However, since the values are lower than unity, radiation is not harmful for people through dermal exposure. The mean estimated total lifetime radiation cancer risk and hereditary effects were 3.44E-04 and 1.18E-09, respectively. The results of total lifetime radiation hereditary effect in all drinking spring waters were less than the recommend acceptable risk value (1.0E-04), while total lifetime radiation cancer risk in all spring waters used for drinking was more than 1.0E-04. The highest cancer risk by radiation was calculated in Yandasht (S11) spring water as 3.54E-04

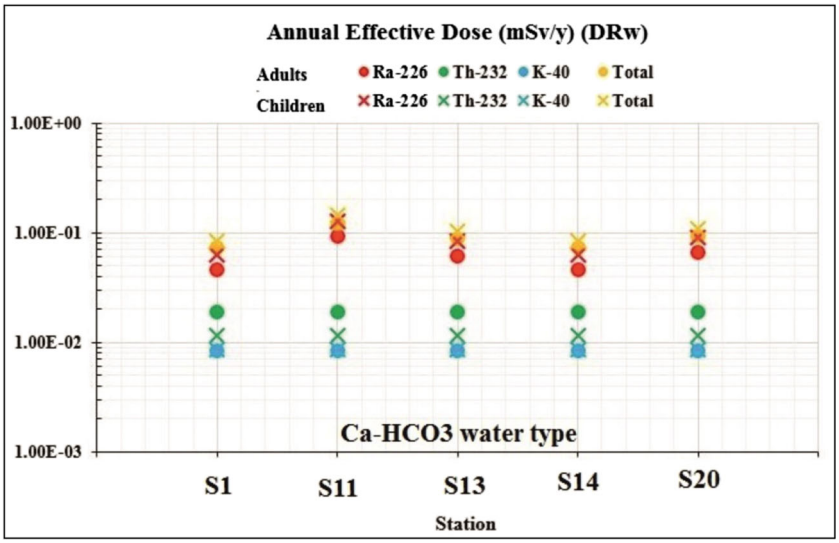

Fig 5 Distributions of annual effective dose (DR_w) for ingestion in children and adults along the sampling stations

(Table S8), implying that approximately 3 out of 10,000 may develop some sort of cancer. However, in order to assess more reliable health risks, some exposure parameters such as the daily intake rate of water, dermal exposure condition, and age of local people should also be considered (USEPA 2004).

Conclusion

The emphasis of the present study was to assess the quality and associated health risks of Na-Cl and Ca-HCO_3 spring water in a high natural background radiation area in North Iran. The results showed that the concentrations of Al, Cd, Cr, Cu, Pb, Mo, Ni, Sb, Zn, and ^{40}K were considerably below the recommended permissible level in all spring waters. Nevertheless, elevated concentrations of As, Mn, Hg, ^{226}Ra, and ^{232}Th were observed in Na-Cl water type, and Fe in Ca-HCO_3 water type. Subsurface thermal processes and mixing of spring water with thermal fluids are assumed to be the main reasons for the measured high concentrations of these elements in the study area. Calculated $HI_{Ingestion}$ and HI_{Dermal} of PTEs are lower than the desirable limit, suggesting low health risk for adults and children. Also, the mean total annual effective doses of radioactive elements were lower than UNSCEAR recommended reference levels for both age groups of population. The most important concern seems to be the spread of toxic elements on the surface via uncontrolled runoffs. Strict control and quarantine measures must be taken to maintain the quality of non-contaminated groundwater and agriculture soil. Moreover, a range of mitigation and adaptation strategies must be followed to avoid contamination through spring water.

Funding information The authors of this paper would like to express their gratitude to Medical Geology Research Center and Radiation Research Center of Shiraz University for financial and logistic supports.

References

Aboyeji OS, Eigbokhan SF (2016) Evaluations of groundwater contamination by leachates around Olusosun open dumpsite in Lagos metropolis, Southwest Nigeria. J Environ Manag 183:333–341

Aghanabati SA (2004) Geological survey of Iran. Geology of Iran. 606 pp. (in Persian).

Ahmad N, ur Rehman J, Rehman J, Nasar G (2019) Effect of geochemical properties (pH, conductivity, TDS) on natural radioactivity and dose estimation in water samples in Kulim. Malaysia Hum Ecol Risk Assess:1–9

Alavi M (1991) Sedimentary and structural characteristics of the Paleo-Tethys remnants in Northeastern Iran. Geol Soc Am Bull 103(8): 983–992

Alavi M (1996) Tectonostratigraphic synthesis and structural style of the Alborz mountain system in Northern Iran. J Geodyn 21(1):1–33

Al-Shboul KF, Alali AE, Batayneh IM, Al-Khodire HY (2017) Radiation hazards and lifetime risk assessment of tap water using liquid scintillation counting and high-resolution gamma spectrometry. J Environ Radioact 178:245–252

Amarouche-Yala S, Benouadah A, el Ouahab BA, Moulla AS, Ouarezki SA, Azbouche A (2015) Physicochemical, bacteriological, and radiochemical characterization of some Algerian thermal spring waters. Expo Health 7(2):233–249

Ansari MR, Ghomi Avili J, Riazian M (2011) Study of environmental chemistry and therapeutic properties of ramsar thermal spring and radiations from thermal springs of the area on the residents. Orient J Chem 27(4):1523–1530

APHA (1995) Standard methods for the examination of water and wastewater, 19th edn.

Arafat AA, Salama MHM, El-Sayed SA, Elfeel AA (2017) Distribution of natural radionuclides and assessment of the associated hazards in

the environment of Marsa Alam-Shalateen area, Red Sea coast, Egypt. J Radiat Res Appl Sci 10(3):219–232
ASTM (2004) Standard practices for the measurement of radioactivity (D3648), Vol. 11.02.
ATSDR (2007) Toxicological profile for arsenic. U.S. Department Of Health And Human Services, Public Health Service Agency for Toxic Substances and Disease Registry, 559.
Bagnato E, Aiuppa A, Parello F, D'Alessandro W, Allard P, Calabrese S (2009) Mercury concentration, speciation and budget in volcanic aquifers: Italy and Guadeloupe (Lesser Antilles). J Volcanol Geotherm Res 179(1-2):96–106
Benedik L, Rovan L, Klemenčič H, Gantar I, Prosen H (2015) Natural radioactivity in tap waters from the private wells in the surroundings of the former Žirovski Vrh uranium mine and the age-dependent dose assessment. Environ Sci Pollut Res 22(16):12,062–12,072
Berberian M (1983) The Southern Caspian: a compressional depression floored by a trapped, modified oceanic crust. Can J Earth Sci 20(2): 163–183
Brookins DG (2012) Eh-pH diagrams for geochemistry. Springer Science & Business Media.
Doroozi R, Vaccaro C, Masoudi F, Petrini R (2016) Cretaceous alkaline volcanism in south Marzanabad, northern central Alborz, Iran: geochemistry and petrogenesis. Geosci Front 7(6):937–951
El-Gamal H, Sidique E, Farid MEA (2018) Considerable radioactivity levels in the granitic rocks of the central areas of the Eastern Desert, Egypt. Environ Sci Pollut Res 25(29):29,541–29,555
El-Mageed AIA, El-Kamel AEH, Abbady AEB, Harb S, Saleh II (2013) Natural radioactivity of ground and hot spring water in some areas in Yemen. Desalination 321:28–31
Fathabadi N, Salehi AA, Naddafi K, Kardan MR, Yunesian M, Nodehi RN, Karimi M (2017) Radioactivity levels in the mostly local foodstuff consumed by residents of the high level natural radiation areas of Ramsar, Iran. J Environ Radioact 169:209–213
Gbadago JK, Faanhof A, Schandorf C, Darko EO, Addo MA (2011) Contributions of natural radionuclides in the domestic water of two critical gold mining communities in Ghana. Expo Health 3(3-4):149–155
Goldhaber SB (2003) Trace element risk assessment: essentiality vs. toxicity. Regul Toxicol Pharmacol 38(2):232–242
Gustin MS, Lindberg SE, Weisberg PJ (2008) An update on the natural sources and sinks of atmospheric mercury. Appl Geochem 23(3): 482–493
Hallberg KB, Johnson DB (2005) Biological manganese removal from acid mine drainage in constructed wetlands and prototype bioreactors. Sci Total Environ 338(1-2):115–124
Holman IP, Allen DM, Cuthbert MO, Goderniaux P (2012) Towards best practice for assessing the impacts of climate change on groundwater. Hydrogeol J 20(1):1–4
Huq ME, Fahad S, Shao Z, Sarven MS, Al-Huqail AA, Siddiqui MH, Rauf A (2019) High arsenic contamination and presence of other trace metals in drinking water of Kushtia district, Bangladesh. J Environ Manag 242:199–209
ICRP (1990) Recommendations of the international commission on radiological protection. ICRP Publication 60.
ICRP (1996) Age-dependent doses to members of the public from intake of radionuclides: part 5. Compilation of ingestion and inhalation dose coefficients. Ann ICRP 26(1):1–91
ICRP (2012) Compendium of dose coeeficients based on ICRP Publication 60 - ICRP 119.
Iyengar MAR (1990) The natural distribution of radium. Environ Behav Radium 1:59–128
Jan AT, Azam M, Siddiqui K, Ali A, Choi I, Haq QMR (2015) Heavy metals and human health: mechanistic insight into toxicity and counter defense system of antioxidants. Int J Mol Sci 16(12):29592–29, 630
Jasik M, Małek S, Żelazny M (2017) Effect of water stage and tree stand composition on spatiotemporal differentiation of spring water chemistry draining Carpathian flysch slopes (Gorce Mts). Sci Total Environ 599-600:1630–1637
Khademi B, Tahsili A (1972) Environmental radioactivity in certain parts of Iran (No. CONF-720805-P1).
Labidi S, Mahjoubi H, Essafi F, Ben Salah R (2010) Natural radioactivity levels in mineral, therapeutic and spring waters in Tunisia. Radiat Phys Chem 79(12):1196–1202
Langmuir D, Herman JS (1980) The mobility of thorium in natural waters at low temperatures. Geochim Cosmochim Acta 44(11):1753–1766
Lien KW, Ling MP, Pan MH (2019) Assessing Japan imported food products radiation doses and exposure risk following the Fukushima nuclear accident. Exposure and Health 1-11.
Meinzer OE (1965) Outline of ground-water hydrology with definition, 71.
Merian E, Anke M, Ihnat M, and Stoeppler M. 2004. Elements and their compounds in the environment: occurrence, analysis and biological relevance (No. Ed. 2). Wiley-VCH Verlag GmbH & Co. KGaA.
Molinari J, Snodgrass WJ (1990) The chemistry and radiochemistry of radium and the other elements of the uranium and thorium natural decay series. Environ Behav Radium 1:11–56
Moore WS, Reid DF (1973) Extraction of radium from natural waters using manganese-impregnated acrylic fibers. J Geophys Res 78(36): 8880–8886
Moore WS, Shaw TJ (1998) Chemical signals from submarine fluid advection onto the continental shelf. J Geophys Res Ocean 103(C10): 21543–21,552
Mortazavi SMJ, Mozdarani H (2013) Non-linear phenomena in biological findings of the residents of high background radiation areas of Ramsar. Int J Radiat Res 11(1):3–9
Muñoz MO, Bhattacharya P, Sracek O, Ramos OR, Aguirre JQ, Bundschuh J, Maity JP (2015) Arsenic and other trace elements in thermal springs and in cold waters from drinking water wells on the Bolivian Altiplano. J S Am Earth Sci 60:10–20
Nicholson K (1993) Geothermal fluids: chemistry and exploration techniques. Springer Science & Business Media.
Papaefthymiou H, Papatheodorou G, Moustakli A, Christodoulou D, Geraga M (2007) Natural radionuclides and ^{137}Cs distributions and their relationship with sedimentological processes in Patras Harbour, Greece. J Environ Radioact 94(2):55–74
Piper A (1953) A graphic procedure for the geo-chemical interpretation of water analysis. USGS Groundwater (Note no. 12).
Rahman MM, Ng JC, Naidu R (2009) Chronic exposure of arsenic via drinking water and its adverse health impacts on humans. Environ Geochem Health 31(1):189–200
Roba CA, Niță D, Cosma C, Codrea V, Olah Ș (2012) Correlations between radium and radon occurrence and hydrogeochemical features for various geothermal aquifers in Northwestern Romania. Geothermics 42:32–46
Robb L (2004) Introduction to ore-forming processes. Blackwell publishing.
Roozitalab MH, Siadat H, Farshad A (2018) The soils of Iran. Springer International Publishing.
Shabana EI, Kinsara AA (2014) Radioactivity in the groundwater of a high background radiation area. J Environ Radioact 137:181–189
Sherif MI, Sturchio NC (2018) Radionuclide geochemistry of groundwater in the Eastern Desert, Egypt. Appl Geochem 93:69–80
Simbahan J, Kurth E, Schelert J, Dillman A, Moriyama E, Jovanovich S, Blum P (2005) Community analysis of a mercury hot spring supports occurrence of domain-specific forms of mercuric reductase. Appl Environ Microbiol 71(12):8836–8845
Singh UK, Ramanathan AL, Subramanian V (2018) Groundwater chemistry and human health risk assessment in the mining region of East Singhbhum, Jharkhand, India. Chemosphere 204:501–513

Sohrabi M, Babapouran M (2005) New public dose assessment from internal and external exposures in low- and elevated-level natural radiation areas of Ramsar, Iran. Int Congr Ser 1276:169–174

Stackelberg PE, Szabo Z, Jurgens BC (2018) Radium mobility and the age of groundwater in public-drinking-water supplies from the Cambrian-Ordovician aquifer system, north-central USA. Appl Geochem 89:34–48

Tirkey P, Bhattacharya T, Chakraborty S, Baraik S (2017) Assessment of groundwater quality and associated health risks: a case study of Ranchi city, Jharkhand. India 5(May):85–100

Torbehbar AK, Liseroudi MH (2015) Geological classification of proposed geothermal areas of Iran. World Geotherm Congr 2015(April):19–25

UNSCEAR (2000) Sources and effects of ionizing radiation (Report to the General Assembly).United Nations, New York.

UNSCEAR (2013) United Nations Scientific Committee on the effects of atomic radiation: sources, effects and risks of ionizing radiation, UNSCEAR 2013, Volume I, 1, 1, 9–10, 66, 88–90.

USEPA (2004) Risk assessment guidance for superfund (RAGS) volume I. Human health evaluation manual H. US Epa, 1(540/R/99/005), 1–156.

USEPA (2010) Integrated Risk Information System (IRIS). United States Environmental Protection Agency. Retrieved from Available online: http//www.Epa.Gov/irris/index.

USEPA (2011) Exposure factors handbook. United States Environmental Protection Agency.

USEPA (2014) Risk assessment guidance for superfund volume I. Human Health Evaluation Manual (Part E Supplemental Guidance for Dermal Risk Assessment). US Environmental Protection Agency, Washington.

USEPA (2016) Integrated Risk Information System (IRIS). United States Environmental Protection Agency, Washington.

Wang Y, Jiao JJ, Zhang K, Zhou Y (2016) Enrichment and mechanisms of heavy metal mobility in a coastal quaternary groundwater system of the Pearl River Delta, China. Sci Total Environ 545-546:493–502

WHO (1984) Guidelines for drinking water quality, values 3; drinking water quality control in small community supplies. WHO, Geneva

WHO (2011) Guidelines for drinking-water quality. WHO Library Cataloguing-in-Publication Data NLM classification: WA 675, Geneva (4th ed.).

WHO (2017) Guidelines for drinking-water quality: fourth edition incorporating the first addendum World Health Organization, 631.